A New Method for Obtaining the Shape Sensitivities of Planar Microstrip Structures by a Full-Wave Analysis

Jan Ureel, *Student Member, IEEE*, and Daniël De Zutter, *Member, IEEE*

Abstract— **We present the principles and the derivation of a new mixed potential integral equation for the derivative of the surface current with respect to a geometrical parameter for planar microstrip structures embedded in a multilayered substrate. This new integral equation is solved together with the original integral equation with the method of moments by using the same set of test and basis functions. Expressions for the matrix elements as a function of the basis and test functions are given. From the geometrical derivatives of the surface currents, geometrical derivatives of the S-parameters are obtained. In the examples a geometrical parameter is swept over some interval, and the derivative, obtained with the new integral equation, is compared with estimates calculated by using finite differences. Very good agreement is found between these estimates.**

I. Introduction

CONSIDERABLE research has been devoted to the full-wave analysis of planar microstrip structures as can be seen from the numerous publications [1]–[4] on this topic. Such a rigorous analysis is very often based on an integral equation formulation, typically solved with the method of moments (MoM). In this paper, we apply the MoM to the mixed potential integral equation (MPIE) formulation of the problem. This problem formulation and solution method is the most efficient for arbitrarily shaped planar geometries embedded in a laterally infinitely extending, stratified medium because only the conducting surfaces are meshed up. From the surface currents on the microstrip, equivalent scattering parameters of the structure are derived.

Recently attention shifted to the inverse problem: the geometrical design of components based on a full-wave electromagnetic simulation [5], [6]. This design can be automated by the application of powerful optimization methods. Such an optimization, for instance, has already been applied for planar devices with the FEM as analysis method [7].

Efficient local optimization techniques rely heavily on the gradient of the objective function [8]. In a general full-wave electromagnetic problem these first derivatives with respect to the geometrical parameters are not readily available. Therefore, one usually resorts to the numerical but inefficient method of taking finite differences. For a circuit with M geometrical design parameters, a forward or backward finite difference estimate requires at least $M+1$ full-wave analyses of the entire problem. Other methods for obtaining this gradient information consist in fitting or interpolating quadratic polynomials to the goal or error function. This involves several repeated analyses of slightly perturbed problems. In [9], e.g., an efficient interpolation method is described for interpolating and approximating the error surface. Gradient information of the objective function is reconstructed by taking partial derivatives of this interpolant, however with a certain loss of accuracy. The approximation of highly nonlinear response curves stirred also considerable interest in neural networks as function approximators [10], [11]. Other techniques [12] exploit the decrease in simulation time when a coarse grid or mesh is used to simulate the circuit. All these techniques have their own merit, but they basically work at the outside of the electromagnetic simulator and are in fact applicable to whatever computationally intensive simulation.

A more problem-oriented approach is described in [13] and [14] for the full-wave optimization of waveguide filters. The key assumption in this work is that simple, analytically known, expressions exist for the admittance matrix of subsections of the waveguide as a function of the geometrical parameters. For an integral equation based full-wave analysis of even simple microstrip discontinuities, this assumption breaks down: no simple analytical expressions exist for the impedance matrix elements. Another important difference is that in integral equation techniques the geometry is meshed, whereas in [13] no meshing of the geometry is needed.

The present paper presents the principles as well as a method for calculating the derivative of the S-parameter with respect to an arbitrary geometrical parameter using the MPIE as a full-wave analysis method. This derivative or shape sensitivity is obtained as a byproduct of the electromagnetic simulation. Through the examples, it will be demonstrated that this derivative is superior with respect to a finite difference estimate. The method has been shown to be valid in the electrostatic case of planar structures [15], [16] and this work is an extension to the full-wave analysis of planar structures. We confine ourselves to the case of microstrip structures analysed with a MPIE but the principles proposed here are directly applicable to, e.g., the analysis of the same structure with an electrical field integral equation (EFIE) or extendible to the analysis of a hybrid structure with microstrip and slot type discontinuities.

Manuscript received February 20, 1995; revised November 12, 1995.

The authors are with Electromagnetics Group, Department of Information Technology (INTEC), University of Gent, St. Pietersnieuwstraat 41, 9000 Gent, Belgium.

Publisher Item Identifier S 0018-9480(96)01448-2.

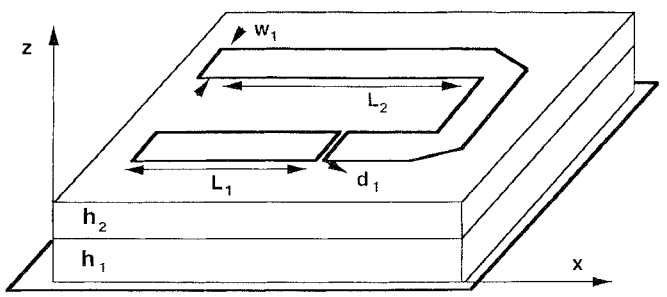

Fig. 1. Example geometry of a planar microstrip structure embedded in a multilayered substrate.

II. Derivation of an Integral Equation for the Total Geometrical Derivative of the Current

A. Geometry and Geometrical Parameters of the Problem

The general geometry of a planar microstrip circuit, embedded in a multilayered substrate is depicted in Fig. 1. The substrate consists of an arbitrary number of layers, stacked in the z-direction. The layers extend to infinity in x- and y-direction. A metallic ground plane and/or top plane can be present. The microstrip circuit consists of thin metallization surfaces of arbitrary shape. The thickness of the metallization is assumed to be negligible in comparison with the layer thicknesses. Losses are modeled by taking a surface impedance of the conductors into consideration. Different types of geometrical parameters appear in this multilayered planar microstrip structure: thicknesses of the substrate layers (such as h_1 and h_2), distances between metallization surfaces (e.g. d_1) and geometrical parameters pertaining to the surface itself like width or length (e.g., L_1, L_2 or w_1). We confine ourselves to the last two types of geometrical parameters. Derivatives with respect to layer thicknesses will be the subject of a forthcoming paper.

B. Integral Equations

The relation between the incident tangential electrical field and the surface current on the microstrip is given by the well-known MPIE [3], [4], [17]

$$\bar{E}^{\text{inc}}(\bar{r}) = Z_s \bar{J}(\bar{r}) + \int_{S_\xi} G^A(\bar{r} \mid \bar{r}')\bar{J}(\bar{r}')dS - \bar{\nabla}\left[\int_{S_\xi} G^V(\bar{r} \mid \bar{r}')\bar{\nabla}' \cdot \bar{J}(\bar{r}')dS\right] \tag{1}$$

where

$\bar{E}^{\text{inc}}(\bar{r})$	the tangential component of the incident electrical field
$\bar{J}(\bar{r})$	the unknown surface current distribution
$G^V(\bar{r} \mid \bar{r}'), G^A(\bar{r} \mid \bar{r}')$	the electrical or magnetic Green's function kernel
Z_s	the surface impedance of the conductor.

This integral equation follows directly from the representation of the electrical field as a function of a magnetic vector potential and an electrical scalar potential and the application of the zero boundary condition for the total electrical field on the conducting surface S_ξ. For simplicity, we assume that ξ represents a single geometrical parameter which modifies the shape of the surface S_ξ in the plane of the surface. Extension to multiple geometrical parameters is straightforward. The total derivative of the surface current with respect to the geometrical parameter ξ is given by

$$\bar{J}_\xi(\bar{r}) = \frac{\partial}{\partial \xi}\bar{J}(\bar{r}) + (\bar{v} \cdot \bar{\nabla})\bar{J}(\bar{r}) \tag{2}$$

with $\bar{v} = d\bar{r}/d\xi$. We call $\bar{v}$ a velocity vector. This vector always lies in the plane of the circuit (i.e., a plane parallel to the (x, y) plane) and describes how an arbitrary position coordinate of the metallization surface changes with ξ. The total derivative consists of two parts: the first part describes the dependence of the surface current on the geometrical parameter itself, and the second part describes the change in current as a consequence of the change in position coordinates. The total derivative of the surface current with respect to the geometrical parameter satisfies the following integral equation

$$\begin{aligned}
&\frac{\partial}{\partial \xi}\bar{E}^{\text{inc}} + (\bar{v} \cdot \bar{\nabla})\bar{E}^{\text{inc}} \\
&\quad = Z_s \bar{J}_\xi + \int_{S_\xi} G^A(\bar{r} \mid \bar{r}')\bar{J}'_\xi dS' \\
&\qquad - \bar{\nabla}\left[\int_{S_\xi} G^V(\bar{r} \mid \bar{r}')(\bar{\nabla}' \cdot \bar{J}'_\xi)dS'\right] \\
&\qquad + \int_{S_\xi} \bar{\nabla}' \cdot [(\bar{v}' - \bar{v})G^A(\bar{r} \mid \bar{r}')]\bar{J}' dS' \\
&\qquad - \bar{\nabla}\left\{\int_{S_\xi} \bar{\nabla}' \cdot [(\bar{v}' - \bar{v})G^V(\bar{r} \mid \bar{r}')](\bar{\nabla}' \cdot \bar{J}')\right. \\
&\qquad\quad + G^V(\bar{r} \mid \bar{r}')\bar{J}' \cdot \bar{\nabla}'(\bar{\nabla}' \cdot \bar{v}') \\
&\qquad\quad \left. - G^V(\bar{r} \mid \bar{r}')\bar{\nabla}' \cdot ((\bar{J}' \cdot \bar{\nabla}')\bar{v}')dS'\right\} \\
&\qquad + (\bar{\nabla}\bar{v}) \cdot \bar{\nabla}\left[\int_{S_\xi} G^V(\bar{r} \mid \bar{r}')\bar{\nabla}' \cdot \bar{J}' dS'\right].
\end{aligned} \tag{3}$$

This new integral equation is obtained by applying the flux-transport theorem on the MPIE (1). For a full derivation of this integral equation, the reader is referred to Appendix A. We denote the explicit dependence of the velocity and surface current on the excitation position vector with the following notations: $\bar{v}' = \bar{v}(\bar{r}')$ and $\bar{J}' = \bar{J}(\bar{r}')$. The first three terms on the right-hand side of (3) are similar to the right-hand side of (1) but with the unknown $\bar{J}'_\xi$ (2) replacing $\bar{J}'$, the next two terms are similar to the second and third term in (1) but in these terms a different "modified" kernel appears of the form $\bar{\nabla}' \cdot [(\bar{v}' - \bar{v})G^V(\bar{r} \mid \bar{r}')]$ or $\bar{\nabla}' \cdot [(\bar{v}' - \bar{v})G^A(\bar{r} \mid \bar{r}')]$. The last three terms stem from the integro-differential character of (1). We will use the following notations to denote the modified kernels

$$\begin{aligned}
R^V(\bar{r} \mid \bar{r}') &= \bar{\nabla}' \cdot [(\bar{v}' - \bar{v})G^V(\bar{r} \mid \bar{r}')] \\
R^A(\bar{r} \mid \bar{r}') &= \bar{\nabla}' \cdot [(\bar{v}' - \bar{v})G^A(\bar{r} \mid \bar{r}')]
\end{aligned} \tag{4}$$

III. Solution of the Integral Equations with the Method of Moments

The two integral (1) and (3) will be solved with the classical method of moments. Therefore, the surface current is expanded in a sum of N basis functions, denoted by $\bar{B}_j(\bar{r}')$

$$\bar{J}' = \sum_{j=1}^{N} I_j \bar{B}_j(\bar{r}') \tag{5}$$

and after testing with N test functions $\bar{T}_i(\bar{r})$ the following system of linear equations from (1) is obtained

$$V_i = Z_{ij} I_j \tag{6}$$

where

$$\begin{aligned} Z_{ij} = Z_s &\int_S \bar{T}_i(\bar{r}) \cdot \bar{B}_j(\bar{r}) dS + \int_S \bar{T}_i(\bar{r}) \\ &\cdot \int_S G^A(\bar{r} \mid \bar{r}') \bar{B}_j(\bar{r}') dS' dS \\ &- \int_S \bar{T}_i(\bar{r}) \cdot \bar{\nabla} \int_S G^V(\bar{r} \mid \bar{r}') \bar{\nabla}' \cdot \bar{B}_j(\bar{r}') dS' dS \end{aligned} \tag{7}$$

$$V_i = \int_S \bar{T}_i(\bar{r}) \cdot \bar{E}^{\text{inc}}(\bar{r}) dS. \tag{8}$$

For simplicity, we will omit the subscript ξ of S_ξ from now on. The solution of the surface current can be found by solving the (6). To solve the second integral equation, we expand the unknown $\bar{J}'_\xi$ over the **same** set of basis functions

$$\bar{J}'_\xi = \sum_{j=1}^{N} I_j^\xi \bar{B}_j(\bar{r}') \tag{9}$$

and substitute the solution of (1), i.e., the approximate surface current distribution (5) in (3). After testing with the **same** test functions, we again obtain a system of linear equations in the unknowns I_j^ξ

$$M_i - W_{ij} I_j = Z_{ij} I_j^\xi \tag{10}$$

where

$$\begin{aligned} W_{ij} = &\int_S \bar{T}_i(\bar{r}) \cdot \int_S R^A(\bar{r} \mid \bar{r}') \bar{B}_j(\bar{r}') dS' dS \\ &- \int_S \bar{T}_i(\bar{r}) \cdot \bar{\nabla} \Big\{ \int_S R^V(\bar{r} \mid \bar{r}') \bar{\nabla}' \cdot \bar{B}_j(\bar{r}') \\ &\quad + G^V(\bar{r} \mid \bar{r}') \bar{B}_j(\bar{r}') . (\bar{\nabla}'(\bar{\nabla}' \cdot \bar{v}')) \\ &\quad - G^V(\bar{r} \mid \bar{r}') \bar{\nabla}' \cdot \left[(\bar{B}_j(\bar{r}') . \bar{\nabla}') \bar{v}' \right] dS' \Big\} dS \\ &+ \int_S \bar{T}_i(\bar{r}) \cdot (\bar{\nabla} \bar{v}) \cdot \bar{\nabla} \left[\int_S G^V(\bar{r} \mid \bar{r}') \bar{\nabla}' \cdot \bar{B}_j(\bar{r}') dS' \right] dS \end{aligned} \tag{11}$$

$$M_i = \int_S \bar{T}_i(\bar{r}) \cdot \left[\frac{\partial \bar{E}^{\text{inc}}}{\partial \xi} + (\bar{v} \cdot \bar{\nabla}) \bar{E}^{\text{inc}} \right] dS. \tag{12}$$

The same impedance matrix Z_{ij} stands before the unknowns I_j^ξ, which is direct consequence of using the same set of basis functions and test functions. If we solve for the surface currents by a LU-decomposition of the system matrix $[Z_{ij}]$ then the solution of the geometrical derivative I_j^ξ only needs N^2 additional computations where N is the number of unknowns. No assumptions have yet been made concerning the nature of basis and test functions: the method can be applied with subsectional or full domain basis funtions, one can choose between the Galerkin solution or a scheme using rooftop functions in conjunction with pointmatching. The only restriction for a computationally efficient method is that the same set of basis and test functions is used for both integral equations. The introduction of the numerical method of moment solution of the surface current implicates a certain error for the geometrical derivative. For a discussion of this approximation and its consequences, we refer the reader to [15].

IV. Derivation of the Matrix Elements

In this section we derive simple expressions for the Z- and W-matrix elements ((7) and (11)) in terms of basis and test functions by eliminating the gradient vectors before the integral sign as it is difficult to handle these numerically. We assume that the geometry is meshed up in a mesh of rectangular or triangular cells and that the test and basis functions used are subsectional.

A. Derivation of the Z-Matrix Elements

By using Green's theorem, the elements of the Z-matrix can be rewritten as

$$\begin{aligned} Z_{ij} = Z_s &\int_S \bar{T}_i(\bar{r}) \cdot \bar{B}_j(\bar{r}) dS + \int_S \bar{T}_i(\bar{r}) \\ &\cdot \int_S G^A(\bar{r} \mid \bar{r}') \bar{B}_j(\bar{r}') dS' dS \\ &- \oint_{\partial S} \bar{T}_i(\bar{r}) G^V(\bar{r} \mid \bar{r}') \bar{\nabla}' \cdot \bar{B}_j(\bar{r}') \cdot \bar{n} dl \\ &+ \int_S \bar{\nabla} \cdot \bar{T}_i(\bar{r}) \int_S G^V(\bar{r} \mid \bar{r}') \bar{\nabla}' \cdot \bar{B}_j(\bar{r}') dS' dS \end{aligned} \tag{13}$$

where $\bar{n}$ is the outside oriented normal unit vector along the boundary ∂S of the surface S. The third term, i.e., the integral over ∂S, disappears because the normal component of the surface current is continuous across two adjacent cells. At the boundary of the surface S, the normal component of the current is zero. Hence, the impedance matrix elements reduce to

$$\begin{aligned} Z_{ij} = Z_s &\int_S \bar{T}_i(\bar{r}) \cdot \bar{B}_j(\bar{r}) dS \\ &+ \int_S \bar{T}_i(\bar{r}) \cdot \int_S G^A(\bar{r} \mid \bar{r}') \bar{B}_j(\bar{r}') dS' dS \\ &+ \int_S \bar{\nabla} \cdot \bar{T}_i(\bar{r}) \int_S G^V(\bar{r} \mid \bar{r}') \bar{\nabla}' \cdot \bar{B}_j(\bar{r}') dS' dS. \end{aligned} \tag{14}$$

The matrix elements Z_{ij} also appear before the unknowns I_j^ξ in (10). The expression for the matrix elements reduces to (14) if we force the normal component of the total derivative of the surface current to be continuous across two adjacent cells. The normal component of the total derivative of the surface current at the boundary of S is usually zero. This can be seen as follows: we denote the surface current at the boundary ∂S_ξ

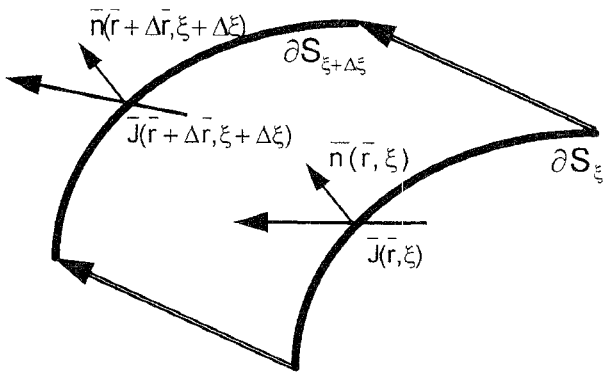

Fig. 2. Condition at the boundary of the surface during parameter variation.

by $\bar{J}(\bar{r},\xi)$. Then, $\bar{J}(\bar{r}+\Delta\bar{r},\xi+\Delta\xi)$ is the surface current at the boundary $\partial S_{\xi+\Delta\xi}$ for a perturbed value of ξ. Remark that when perturbing ξ the position $\bar{r}$ on the boundary changes to $\bar{r}+\Delta\bar{r}$. If we consider the normal component of the surface current, one can state that for every $\Delta\xi$ (see Fig. 2)

$$\frac{\bar{J}(\bar{r}+\Delta\bar{r},\xi+\Delta\xi)\cdot\bar{n}(\bar{r}+\Delta\bar{r},\xi+\Delta\xi)-\bar{J}(\bar{r},\xi)\cdot\bar{n}(\bar{r},\xi)}{\Delta\xi}=0 \tag{15}$$

because before and after shape variation the normal component of the surface current is zero. If the unit normal vector stays constant during the parameter variation, i.e. $\bar{n}(\bar{r},\xi)=\bar{n}(\bar{r}+\Delta\bar{r},\xi+\Delta\xi)$ for all $\Delta\xi$, then

$$\frac{\bar{J}(\bar{r}+\Delta\bar{r},\xi+\Delta\xi)-\bar{J}(\bar{r},\xi)}{\Delta\xi}\cdot\bar{n}(\bar{r},\xi)=0 \tag{16}$$

or when taking the limit

$$\left[\frac{\partial}{\partial\xi}\bar{J}(\bar{r})+(\bar{v}\cdot\bar{\nabla})\bar{J}(\bar{r})\right]\cdot\bar{n}(\bar{r},\xi)=0. \tag{17}$$

Hence one can conclude that in (10) the expression for the Z_{ij} reduces to (14), on the condition that the normal unit vector stays the same during parameter variation. This will be the case taking into consideration the assumptions which will be made in the following Section IV-B.

B. Derivation of the W-Matrix Elements

Following the same method, we will try to eliminate the gradient vectors before the integral sign in (11). To simplify (11), we make the following basic assumption: the velocity vector is a piecewise continuous vector field with support on S. In each part of S (this could be in each cell), the velocity vector can be written in the standard form

$$\bar{v}=[\alpha_x x+\beta_x y+\gamma_x]\bar{u}_x+[\alpha_y x+\beta_y y+\gamma_y]\bar{u}_y \tag{18}$$

where $\bar{u}_x$ and $\bar{u}_y$ are the unit vectors in x- and y-direction. Parts of the surface S can only undergo linear transformations: expansion, contraction or translation, in other words all deformations where the congruency with the original surface is maintained are admissible. Non-linear deformations however can not be handled through this standard form. This basic assumption allows us to considerably simplify the integral (3) and the matrix elements in (11) without too severely restricting the generality of possible modifications of the shape of the surface. As a consequence of (18), the normal unit vector $\bar{n}(\bar{r},\xi)$ will also remain constant during deformation, automatically leading to (17).

As a direct consequence of this basic assumption, the term in (11) with $\bar{\nabla}'(\bar{\nabla}'\cdot\bar{v}')$ disappears because this factor is zero on the entire surface.

The remaining terms of the W-matrix elements

$$-\int_S\bar{T}_i(\bar{r})\cdot\bar{\nabla}\left\{\int_S R^V(\bar{r}\mid\bar{r}')\bar{\nabla}'\cdot\bar{B}_j(\bar{r}')-G^V(\bar{r}\mid\bar{r}')\bar{\nabla}'\cdot[(\bar{B}_j(\bar{r}')\cdot\bar{\nabla}')\bar{v}']dS'\right\}dS \tag{19}$$

and

$$\int_S\bar{T}_i(\bar{r})\cdot(\bar{\nabla}\bar{v})\cdot\bar{\nabla}\left\{\int_S G^V(\bar{r}\mid\bar{r}')\bar{\nabla}\cdot\bar{B}_j(\bar{r}')dS'\right\}dS \tag{20}$$

will be handled separately. By applying Green's theorem to (19), we get

$$\begin{aligned}&-\oint_{\partial S}\bar{T}_i(\bar{r})\cdot\int_S R^V(\bar{r}\mid\bar{r}')\bar{\nabla}'\cdot\bar{B}_j(\bar{r}')dS'\bar{n}dl\\&+\oint_{\partial S}\bar{T}_i(\bar{r})\cdot\int_S G^V(\bar{r}\mid\bar{r}')\bar{\nabla}'\cdot[(\bar{B}_j(\bar{r}')\cdot\bar{\nabla}')\bar{v}']dS'\bar{n}dl\\&+\int_S\bar{\nabla}\cdot\bar{T}_i(\bar{r})\int_S R^V(\bar{r}\mid\bar{r}')\bar{\nabla}'\cdot\bar{B}_j(\bar{r}')dS'dS\\&-\int_S\bar{\nabla}\cdot\bar{T}_i(\bar{r})\int_S G^V(\bar{r}\mid\bar{r}')\bar{\nabla}'\cdot[(\bar{B}_j(\bar{r}')\cdot\bar{\nabla}')\bar{v}']dS'dS.\end{aligned} \tag{21}$$

The contour integrals are taken along the boundary of the surface S. Because the normal component of the surface currents I_j are continuous across two cell boundaries, only two terms of (19) remain

$$\int_S\bar{\nabla}\cdot\bar{T}_i(\bar{r})\int_S\{R^V(\bar{r}\mid\bar{r}')\bar{\nabla}'\cdot\bar{B}_j(\bar{r}')-G^V(\bar{r}\mid\bar{r}')\bar{\nabla}'\cdot[(\bar{B}_j(\bar{r}')\cdot\bar{\nabla}')\bar{v}']\}dS'dS. \tag{22}$$

We can rewrite the term $\bar{\nabla}'\cdot[(\bar{B}_j(\bar{r}')\cdot\bar{\nabla}')\bar{v}']$ by substituting the canonical form for the velocity $\bar{v}$ (18)

$$\bar{\nabla}'\cdot[(\bar{B}_j(\bar{r}')\cdot\bar{\nabla}')\bar{v}']=\alpha_x\frac{\partial B_{jx}}{\partial x'}+\beta_x\frac{\partial B_{jy}}{\partial x'}+\alpha_y\frac{\partial B_{jx}}{\partial y'}+\beta_y\frac{\partial B_{jy}}{\partial y'}. \tag{23}$$

We also substitute (18) into (20) and if we denote the "potential" due to a single basis function $\bar{B}_j(\bar{r}')$ by $\phi_j(\bar{r})$

$$\phi_j(\bar{r})=\int_S G^V(\bar{r}\mid\bar{r}')\bar{\nabla}'\cdot\bar{B}_j(\bar{r}')dS' \tag{24}$$

then

$$[\bar{\nabla}\bar{v}]\cdot\bar{\nabla}\phi_j(\bar{r})=\left[\alpha_x\frac{\partial\phi_j}{\partial x}+\alpha_y\frac{\partial\phi_j}{\partial y}\right]\bar{u}_x+\left[\beta_x\frac{\partial\phi_j}{\partial x}+\beta_y\frac{\partial\phi_j}{\partial y}\right]\bar{u}_y. \tag{25}$$

Denoting the test function $\bar{T}_i(\bar{r})$ by $T_{ix}\bar{u}_x + T_{iy}\bar{u}_y$, (20) becomes

$$\begin{aligned}\int_S \bar{T}_i(\bar{r})\cdot(\bar{\nabla}\bar{v})\cdot\bar{\nabla}\phi_j dS &= \int_S \left[T_{ix}\left(\alpha_x\frac{\partial\phi_j}{\partial x}+\alpha_y\frac{\partial\phi_j}{\partial y}\right)\right. \\ &\quad \left. +T_{iy}\left(\beta_x\frac{\partial\phi_j}{\partial x}+\beta_y\frac{\partial\phi_j}{\partial y}\right)\right]dS \qquad (26)\\ &= \int_S \left[\frac{\partial}{\partial x}(\alpha_x T_{ix}\phi_j+\beta_x T_{iy}\phi_j)\right. \\ &\quad +\frac{\partial}{\partial y}(\alpha_y T_{ix}\phi_j+\beta_y T_{iy}\phi_j) \\ &\quad -\alpha_x\frac{\partial T_{ix}}{\partial x}\phi_j-\alpha_y\frac{\partial T_{ix}}{\partial y}\phi_j \\ &\quad \left.-\beta_x\frac{\partial T_{iy}}{\partial x}\phi_j-\beta_y\frac{\partial T_{iy}}{\partial y}\phi_j\right]dS. \qquad (27)\end{aligned}$$

Again using Green's theorem, the first part of (27) can be rewritten as

$$\oint_{\partial S} -(\alpha_y T_{ix}\phi_j+\beta_y T_{iy}\phi_j)dx+(\alpha_x T_{ix}\phi_j+\beta_x T_{iy}\phi_j)dy. \qquad (28)$$

Or if we define a "modified" test function as

$$\bar{\Theta}_i(\bar{r}) = [\alpha_y T_{ix}+\beta_y T_{iy}]\bar{u}_x+[\alpha_x T_{ix}+\beta_x T_{iy}]\bar{u}_y \qquad (29)$$

then (28) is equal to

$$\oint_{\partial S}\bar{\Theta}_i\cdot\int_S G^V(\bar{r}\mid\bar{r}')\bar{\nabla}'\cdot\bar{B}_j(\bar{r}')dS'\bar{n}dl. \qquad (30)$$

The second part of (27) is nothing else than the expansion of $\bar{\nabla}\cdot[(\bar{T}_i(\bar{r})\cdot\bar{\nabla})\bar{v}]$

$$-\int_S\bar{\nabla}\cdot[(\bar{T}_i(\bar{r})\cdot\bar{\nabla})\bar{v}]\int_S G^V(\bar{r}\mid\bar{r}')\bar{\nabla}'\cdot\bar{B}_j(\bar{r}')dS'dS. \qquad (31)$$

Summarizing, we get the following result for the W-matrix elements by summation of all contributions

$$\begin{aligned}W_{ij} &= \int_S\bar{T}_i(\bar{r})\cdot\int_S R^A(\bar{r}\mid\bar{r}')\bar{B}_j(\bar{r}')dS'dS \\ &\quad +\int_S\bar{\nabla}\cdot\bar{T}_i(\bar{r})\int_S R^V(\bar{r}\mid\bar{r}')\bar{\nabla}'\cdot\bar{B}_j(\bar{r}')dS'dS \\ &\quad -\int_S\bar{\nabla}\cdot\bar{T}_i(\bar{r})\int_S G^V(\bar{r}\mid\bar{r}')\bar{\nabla}' \\ &\quad \cdot[(\bar{B}_j(\bar{r}')\cdot\bar{\nabla}')\bar{v}']dS'dS-\int_S\bar{\nabla} \\ &\quad \cdot[(\bar{T}_i(\bar{r})\cdot\bar{\nabla})\bar{v}]\int_S G^V(\bar{r}\mid\bar{r}')\bar{\nabla}'\cdot\bar{B}_j(\bar{r}')dS'dS \\ &\quad +\oint_{\partial S}\bar{\Theta}_i\cdot\int_S G^V(\bar{r}\mid\bar{r}')\bar{\nabla}'\cdot\bar{B}_j(\bar{r}')\bar{n}dS'dl. \qquad (32)\end{aligned}$$

V. Calculation of the Matrix Elements

A. Calculation of the Locally Modified Green's Function

The original integral kernels $G^V(\bar{r}\mid\bar{r}')$ and $G^A(\bar{r}\mid\bar{r}')$ are only a function of $\rho=|\bar{r}'-\bar{r}|$. The kernels $R^V(\bar{r}\mid\bar{r}')$ and $R^A(\bar{r}\mid\bar{r}')$ are functions of $\bar{r}$ and $\bar{r}'$. The analytical expression as a function of ρ of the original potential kernels ($G^V(\bar{r}\mid\bar{r}')$ and $G^A(\bar{r}\mid\bar{r}')$) for an arbitrarily multilayered medium is not known. The kernels are expanded in a Laurent series of ρ over some ρ-interval as in [4]

$$G^X(\rho)=\sum_{k=-1}^{N_{\text{pow}}}c_k^X\rho^k \qquad (33)$$

with $X=A$ or V. The gradient vector of $G^X(\rho)$ with respect to the excitation coordinates is given by

$$\bar{\nabla}'G^X(\rho)=(\bar{r}'-\bar{r})\left[\sum_{k=-1}^{N_{\text{pow}}}kc_k^X\rho^{k-2}\right]. \qquad (34)$$

Taking into account the form of the velocity vector, we can write the locally perturbed Green's function kernels as

$$\begin{aligned}&R^X(\bar{r}\mid\bar{r}') \\ &\quad=\bar{\nabla}'\cdot\bar{v}'G^X(\bar{r}\mid\bar{r}')+(\bar{v}'-\bar{v})\cdot\bar{\nabla}'\cdot G^X(\bar{r}\mid\bar{r}') \\ &\quad=(\alpha_x'+\beta_y')\sum_{k=-1}^{N_{\text{pow}}}c_k^X\rho^k \\ &\qquad+\{\alpha_x'x'(x'-x)+\beta_x'y'(x'-x)-\alpha_x x(x'-x) \\ &\qquad\quad-\beta_x y(x'-x)+(\gamma_x'-\gamma_x)(x'-x) \\ &\qquad\quad+\alpha_y'x'(y'-y)+\beta_y'y'(y'-y) \\ &\qquad\quad-\alpha_y y(y'-y)-\beta_y y(y'-y) \\ &\qquad\quad+(\gamma_y'-\gamma_y)(y'-y)\}\sum_{k=-1}^{N_{\text{pow}}}kc_k^X\rho^{k-2} \qquad (35)\end{aligned}$$

where the coefficients with/without prime belong to excitation/observation cell. For each part of the surface where the excitation and observation velocity coincide ($\bar{v}=\bar{v}'$), (35) simplifies to

$$\begin{aligned}&=(\alpha_x'+\beta_y')\sum_{k=-1}^{N_{\text{pow}}}c_k^X\rho^k \\ &\quad+\{\alpha_x'(x'-x)^2+(\beta_x'+\alpha_y')(y'-y)(x'-x) \\ &\qquad+\beta_y'(y'-y)^2\}\sum_{k=-1}^{N_{\text{pow}}}kc_k^X\rho^{k-2}. \qquad (36)\end{aligned}$$

From (36) we observe that if k equals -1, the singularity of the kernel is of the same order as in the original integral equation, namely a ρ^{-1} term. As a consequence, weak singular integrals of the same type as in the Z-matrix elements appear during calculation of the W-matrix elements.

B. Calculation of the Matrix Elements

For the basis functions and test functions, the classical rooftop functions are used. This corresponds with the Galerkin solution method. Basically the calculation of the matrix elements reduces to the integration of a quadruple integral over excitation and observation cell of a power of ρ and a polynomial function in x, x', y or y'. The integration method used is the same as in [4].

VI. Geometrical Derivative of the Current

If no external incident field is present, then the systems of linear equations reduce to

$$0 = Z_{ij} I_j \tag{37}$$

and

$$0 = Z_{ij} I_j^{\xi} + W_{ij} I_j. \tag{38}$$

In order to calculate circuit parameters, like the Y-Z or S-parameters, port lines are added to the planar structure. At the end of port line, a source excites the structure. If we group the current variables corresponding with the end of the port in the vector I_P and the remaining variables (circuit + rest of port line) in the vector I_S we can rewrite (37) as

$$\begin{bmatrix} 0 \\ 0 \end{bmatrix} = \begin{bmatrix} Z_{SS} & Z_{SP} \\ Z_{PS} & Z_{PP} \end{bmatrix} \begin{bmatrix} I_S \\ I_P \end{bmatrix} \tag{39}$$

with solution

$$I_S = -[Z_{SS}]^{-1}[Z_{SP} I_P]. \tag{40}$$

For the system (38) an analoguous reasoning leads to

$$\begin{bmatrix} 0 \\ 0 \end{bmatrix} = \begin{bmatrix} Z_{SS} & Z_{SP} \\ Z_{PS} & Z_{PP} \end{bmatrix} \begin{bmatrix} I_S^{\xi} \\ I_P^{\xi} \end{bmatrix} + \begin{bmatrix} W_{SS} & W_{SP} \\ W_{PS} & W_{PP} \end{bmatrix} \begin{bmatrix} I_S \\ I_P \end{bmatrix}. \tag{41}$$

Because the source is independent of the geometry, I_P^{ξ} vanishes and the solution for I_P^{ξ} becomes

$$I_S^{\xi} = -Z_{SS}^{-1}[W_{SS} I_S + W_{SP} I_P]. \tag{42}$$

The same inverse matrix is used as in the previous system, which means that only N^2 additional computations are needed in order to solve for the derivative with respect to a geometrical parameter.

VII. Geometrical Derivative of the S-Parameters

The surface density currents at the port or feed lines give rise to the longitudinal currents at each port. Likewise the geometrical derivatives of the surface currents can be easily related to the geometrical derivative of the longitudinal current at the port line. Voltages at each port line are defined by using a power-current definition [18] in the following way: the cross power $P_{p,q}$, injected or reflected at port p, due to a current excitation at port q (other ports open) is defined as

$$P_{p,q} = -\frac{1}{2} \int_{S_p} \bar{E}_{p,q} \cdot \bar{J}_{p,q}^* dS \tag{43}$$

where $\bar{E}_{p,q}$ is the tangential electrical field at port p, $\bar{J}_{p,q}$ the corresponding surface current and S_p the port region. Using a circuit definition, voltages at each port are calculated as

$$V_{p,q} = \frac{2P_{p,q}}{I_{p,q}^*} \tag{44}$$

where $I_{p,q}^*$ is the longitudinal current at port p. Because the applied source current distribution $\bar{J}_{p,q}$ is independent of the geometrical parameters, the derivative of the cross power is given by

$$\frac{\partial P_{p,q}}{\partial \xi} = -\frac{1}{2} \int_{S_p} \left[\frac{\partial}{\partial \xi} \bar{E}_{p,q} + (\bar{v} \cdot \bar{\nabla}) \bar{E}_{p,q} \right] \cdot \bar{J}_{p,q}^* dS. \tag{45}$$

To simplify the discussion, we made the assumption that the port region S_p is independent of the geometrical parameter ξ. This means that derivatives with respect to the width of the port lines cannot be calculated with the method described above. The derivative of the cross power can also be expressed as a function of the calculated I_{ξ} and the matrix elements W_{ij}. Substituting (45) in the derivative of the circuit definition (44), derivatives of the port voltages with respect to the geometrical parameters are obtained as

$$\frac{\partial V_{p,q}}{\partial \xi} = \frac{2}{I_{p,q}^*} \frac{\partial P_{p,q}}{\partial \xi}. \tag{46}$$

From the currents, the geometrical derivatives of the currents, the voltages and the geometrical derivatives of the voltages, the S-parameters and its geometrical derivatives are easily obtained.

VIII. Numerical Examples

The previous theory has been implemented for structures consisting of rectangular cells where the cell dimension can be of different size. We emphasize however that the above theory is not restricted to this type of mesh but could also be implemented for a mixed mesh of rectangles and triangles, however with more numerical efforts.

Some numerical examples will be given where a single geometrical parameter is varied over some interval. As a reference we will calculate an estimate of the derivative of the S-parameter obtained by taking finite differences with a simple four point formula

$$f'(x) = \frac{f(x-2h) - 8f(x-h) + 8f(x+h) - f(x+2h)}{12h} + O(h^4). \tag{47}$$

To this end the integral (3) must be solved four times, each time for a different S_{ξ} surface. This estimate, abbreviated FDD (finite difference derivative) will be sufficiently accurate if the step size h is kept small. The derivative, obtained by solving the integral (3) is called the IED (integral equation derivative). A comparison between these two estimates is made by considering the following relative error measure

$$E_{\text{rel}} = \frac{\left| F\left[\left(\frac{dS_{ij}}{d\xi}\right)_{\text{IED}}\right] - F\left[\left(\frac{dS_{ij}}{d\xi}\right)_{\text{FDD}}\right] \right|}{\left| F\left[\left(\frac{dS_{ij}}{d\xi}\right)_{\text{FDD}}\right] \right|} \tag{48}$$

where $F[\cdot]$ stands for the real part, the imaginary part, the phase or the absolute value and where S_{ij} is one of the S-parameters. A large error can indicate an incorrect IED or a less accurate FDD. The accuracy of the FDD can be arbitrarily increased in theory by decreasing the step size, in practice by using a higher-order formula.

A important issue is still left untouched: if a geometrical parameter which relates to the surface itself (length, width, but not the distance between two surfaces) is changed then the meshing of the structure must be adapted. The manner in which this is performed is arbitrary and must be specified by the user: cells can be added in the meshing, some cells can be expanded or reduced or a combination of both approaches can be used. In the examples presented below, the mesh of the entire structure is changed proportionally with the change of the geometrical parameter. This can be done because all cells are simply rectangles. Such strategy of mesh-adaptation is called the "moving mesh strategy." The opposite is a strategy where the cell-size is restricted to some maximum value and where cells are added. Such strategy is called "the fixed mesh strategy." We always use a "moving mesh strategy," except where mentioned. For a detailed discussion of both strategies and their consequences, we refer the reader to [15].

A. Example 1: Double Stub

We consider a transmission line with two parallel stubs on an alumina substrate ($\epsilon_r = 9.6$, thickness 0.635 mm) (see Fig. 3). The stubs have the same length L and change simultaneously. The width W of the transmission line and stubs is 0.635 mm. We vary the length L from 0.3175 to 3.4925 mm in steps of 0.3175 mm. The operating frequency is 10.0 GHz and the electrical wavelength in the substrate is 11.7 mm. There are two surfaces of which the shape is modified. The different velocity vectors are defined in terms of the same geometrical parameter L as

$$\bar{v}_{\text{stubup}} = \left(\frac{y - W}{L}\right)\bar{u}_y \tag{49}$$

for the first stub and

$$\bar{v}_{\text{stubdown}} = \frac{y}{L}\bar{u}_y \tag{50}$$

for the second stub. On Fig. 3 the meshed geometry and all relevant geometrical data are depicted for three situations during the parameter sweep. The simulated results under the form of the real and imaginary part of the transmission coefficient S_{21} as a function of L for a frequency of 10 GHz are shown in Fig. 4. The correspondence between the finite difference estimate S_{21}^{FDD} and its integral equation counterpart S_{21}^{IED} is determined by taking the relative error of the real and imaginary part according to (48). The results are shown in Fig. 5. The maximum relative error is 1.0% both for the imaginary and real part, which is a very good agreement. A detailed comparison of the CPU-time in seconds, needed for the calculation of S-parameters for one frequency point with geometrical derivatives and the calculation without is made in Table I. The total time is subdivided in the calculation of the quadruple integrals, the calculation of all impedances,

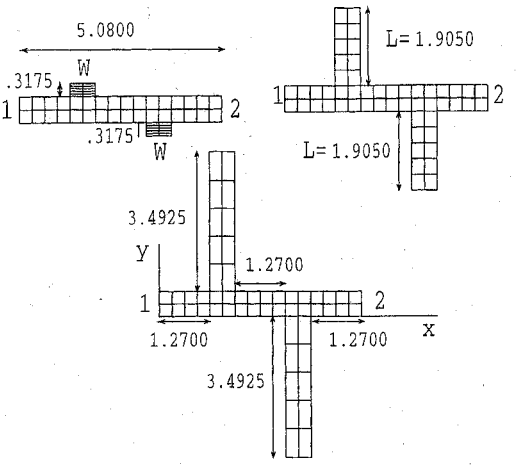

Fig. 3. Geometry and meshing of the double stub example.

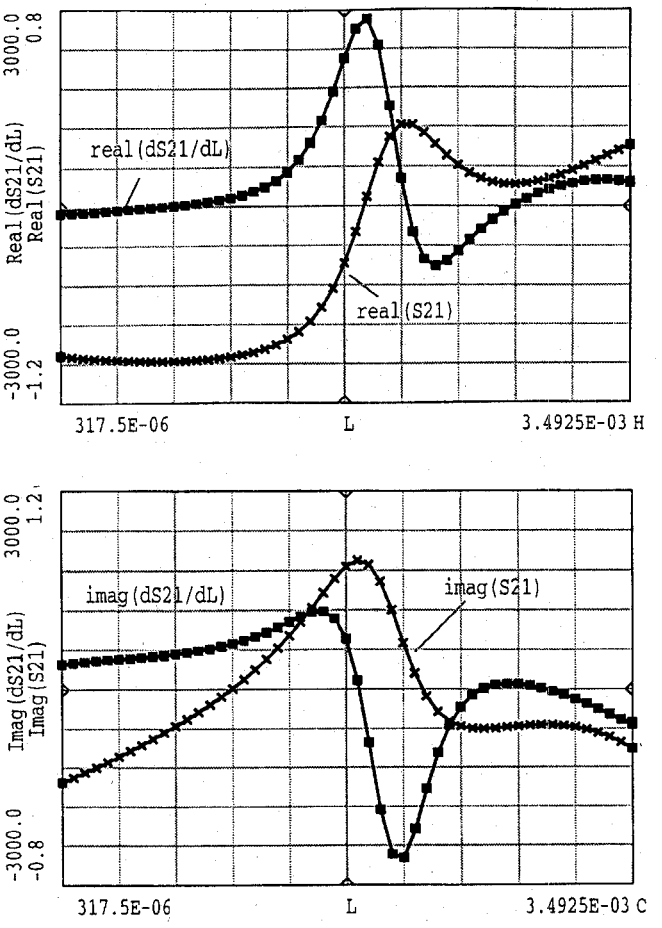

Fig. 4. Real and imaginary part of the transmission coefficient and of the geometrical derivative of the transmission coefficient at 10 GHz for the double stub case.

the assembling and solution of the impedance matrix $[Z_{ij}]$, assembling and solution for the geometrical derivatives of the surface currents and the characterization of the port lines. The time needed for the quadruple integrals triples as compared to the calculation without derivatives because different types of quadruple integrals must be calculated. The time for solving $[Z_{ij}]$ also doubles because a LU-decomposition is performed instead of a symmetric Gauss-elimination method. The time for

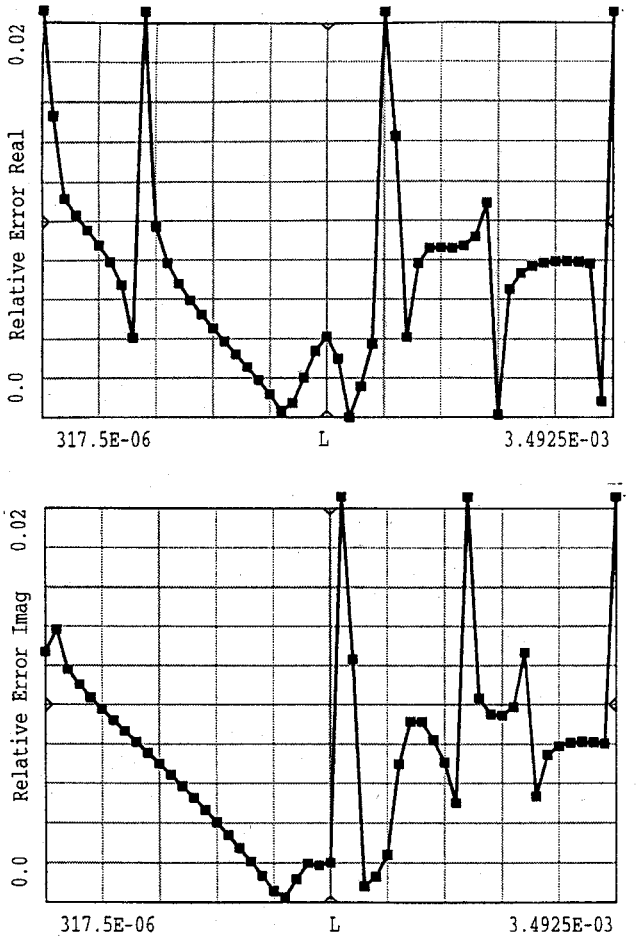

Fig. 5. Relative error between the integral equation derivative and finite difference derivative of the real and imaginary part of the transmission coefficient at 10 GHz for the double stub case.

TABLE I
DETAILED COMPARISON OF THE CPU-TIME IN SECONDS BETWEEN CALCULATION OF S-PARAMETERS WITH GEOMETRICAL DERIVATIVES AND WITHOUT

	with	without
Calculation of Integrals	60	20
Calculation of impedances	10	5
Assemble/Solve Z_{ij}	6	3
Assemble/Solve W_{ij}	0	-
Portlines	6	3
Total time (1 frequency)	82	31
Total time (3 frequencies)	138	61

assembling and solving the $[W_{ij}]$ is, as predicted, negligible. It must be pointed out that this comparison is a worst case comparison: as more frequency points are needed and more geometrical parameters are varied, the calculation time for the case "with" will decrease more as compared to the case "without" (see the last entry in Table I).

B. Example 2: Floating Line Resonator

In [19] a floating line resonator is investigated: two transmission lines are separated by a gap and a small patch. The

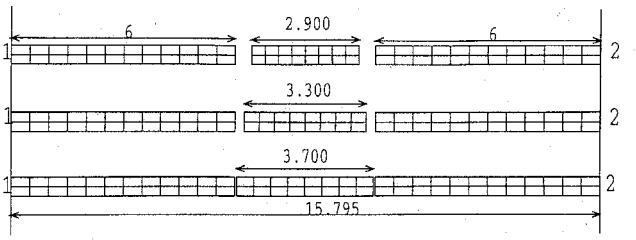

Fig. 6. Geometry and meshing of the floating line resonator example.

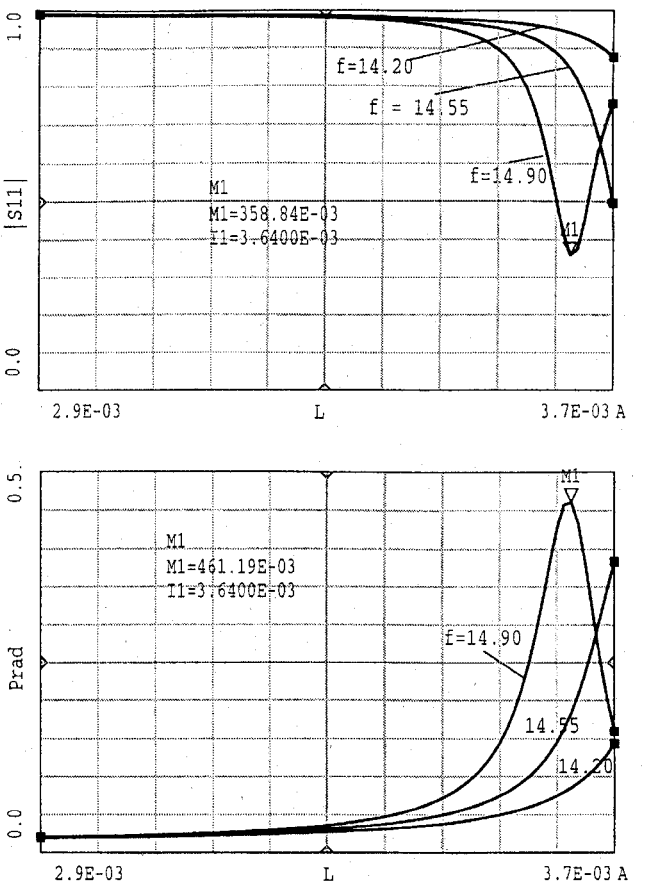

Fig. 7. Reflection coefficient and radiated power of the floating line resonator at different frequencies. Resonance occurs at $L = 3.64$ mm for 14.90 GHz.

circuit lies on substrate with $\epsilon_r = 8.875$ and a thickness of 0.635 mm. At low frequencies this structure can already radiate a substantial part of the injected power. The geometry and mesh of the structure are depicted in Fig. 6 where all dimensions are given in mm. The width of the transmission lines is 0.508 mm. The length L of the resonator patch is varied from 2.90 mm to 3.70 mm with a step size of 0.01 mm. We consider three frequencies 14.20, 14.55, and 14.90 GHz. On Fig. 7 the amplitude of the reflection coefficient S_{11} and the radiated power are shown as a function of the length L for different frequencies. A resonance occurs for $L = 3.635$ mm at a frequency of 14.90 GHz where 45% of the delivered power is radiated. The maximum relative error of real and imaginary part for this case was 0.08%. The availibility of the geometrical derivative allows us to calculate some sensitivity

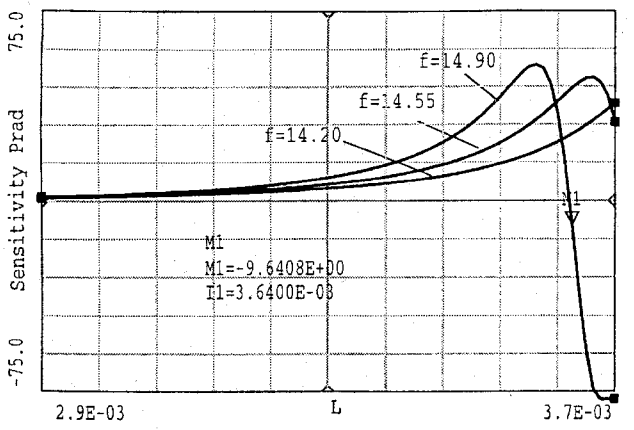

Fig. 8. Sensitivity of the radiated power as a function of the length L for different frequencies (floating line resonator).

measures, for example the relative sensitivity of the radiated power with respect to L is defined as

$$S^{L}_{P_{\text{rad}}} = \frac{dP_{\text{rad}}}{dL}\frac{L}{P_{\text{rad}}} \tag{51}$$

where

$$\frac{dP_{\text{rad}}}{dL} = -2\,\text{Re}\left[\frac{dS_{11}}{dL}S^{*}_{11}\right] - 2\,\text{Re}\left[\frac{dS_{21}}{dL}S^{*}_{21}\right]. \tag{52}$$

This sensitivity measure is shown in Fig. 8 for the executed parameter sweep.

C. Example 3: Five Turn Meander Line

As a last example we consider a meander line with five full turns and arms of equal length L. The meander line lies on a GaAs substrate ($\epsilon_r = 12.85$, thickness 100 μm) and the width of the line is 75 μm. The parameter L is swept from 25 μm until 650 μm with a step size of 2.5 μm for a frequency of 38.0 GHz. The geometry and the meshing are shown in Fig. 9. The velocity vector is chosen in much the same way as in the double stub case. To give an idea, a vector plot of the velocity vector is presented in Fig. 10. At each turn the velocity equals one, while at the center of the structure, the vector is set to zero. Fig. 11 shows the real part and the derivative of the real part of S_{11} with respect to L. On this figure both the IED and FDD are displayed but no difference is visible. Similar results are found for the imaginary part. As the real part of S_{11} possesses a large number of extrema, we have displayed the absolute error between the real part of the IED and the FDD in Fig. 12. The absolute error is sufficiently small (maximum deviation is 300, total variation of the curve in Fig. 11 is 40 000). This result was obtained with a moving mesh strategy: the cell dimension is proportionally adapted with the length. We also performed the same parameter sweep with a fixed mesh strategy. In that case, the mesh generator decides autonomously on the basis of the electrical wavelength at the highest frequency if cells should be added or not. At some values of L, cells will be added. On Fig. 13 the absolute error between the real part of the IED and the FDD is shown for the calculation based on the fixed mesh strategy.

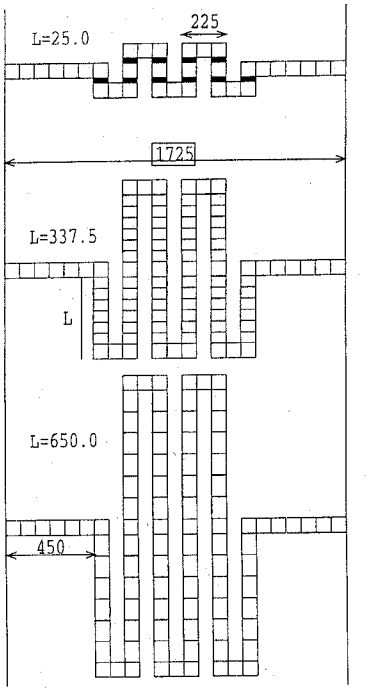

Fig. 9. Geometry of the five turn meander line example.

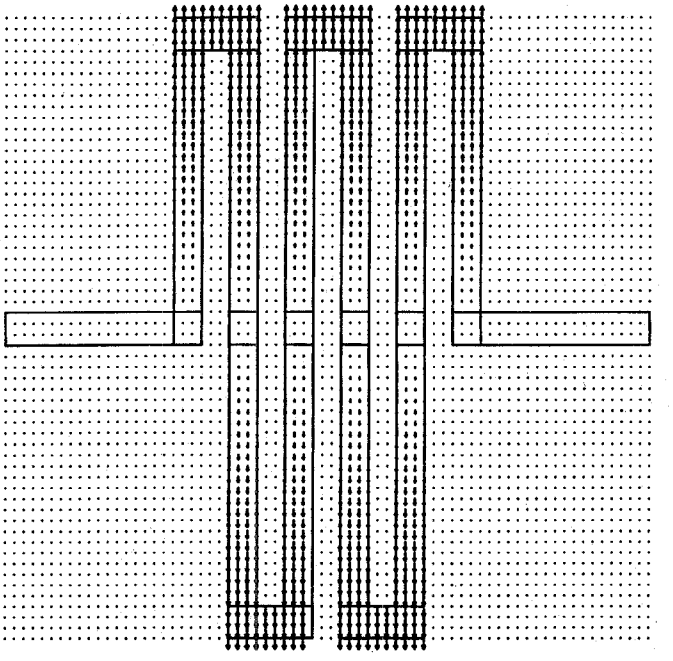

Fig. 10. Velocity vector field for the five turn meander line example.

Relatively large jumps occur in this absolute error which come from the FDD. These jumps coincide with an increase in the number of cells. For example, the first jump in the error curve comes from a change in the number of cells from 44 to 54, the second from a change from 54 to 64, and so on. These discontinuities are due to the fact that two S-parameters, simulated with different discretizations are subtracted from each other. Remark that even with a four-point formula for the finite difference estimate, these jumps are relatively large: near $L = 650$ μm the real part is about $-12\,000$ where the FDD

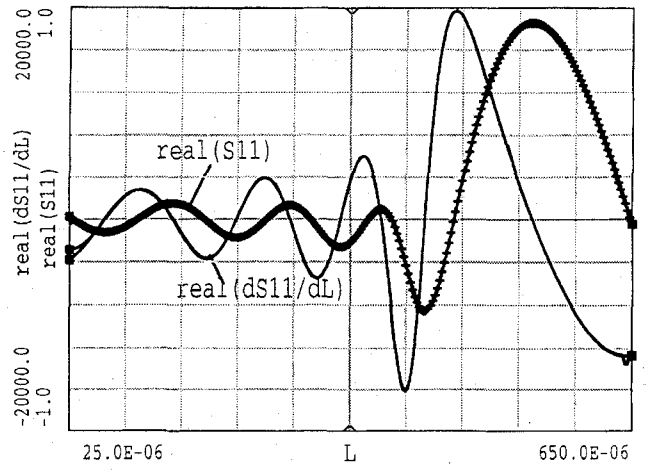

Fig. 11. Real part of the reflection coefficient (moving mesh strategy).

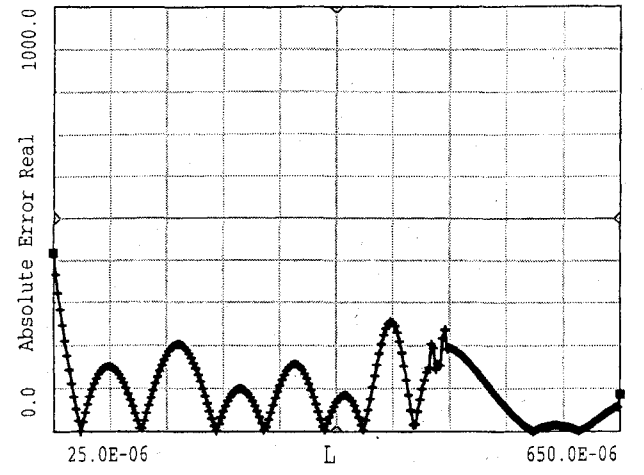

Fig. 12. Absolute error between the integral equation derivative and the finite difference derivative of the real part of the reflection coefficient with a moving mesh strategy.

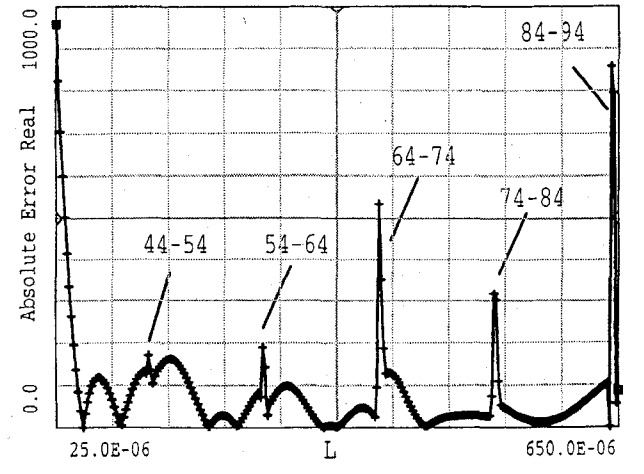

Fig. 13. Absolute error between the integral equation derivative and a finite difference derivative of the real part of the reflection coefficient with a fixed mesh strategy.

predicts a value of $-13\,000$ or a deviation with nearly 10%. Remark also that for this structure consisting of rectangular regions it could be fairly simple to predict these increases in number of cells but for an arbitrary shaped circuit this would be nearly impossible. The IED however always shows a smooth continuous behavior. In this way the IED is superior to a finite difference estimate.

IX. Conclusion

The underlying principles and the derivation of a new integral equation for the total derivative of the surface current with respect to a geometrical parameter were presented. By expanding the unknown total derivative of the current over the same set of basis and test functions as the current, a numerically efficient computation of the geometrical derivative becomes possible as a byproduct of the electromagnetic simulation. An extension of the calibration and deembedding scheme also allows to calculate the S-parameters with respect to a geometrical parameter. Only one meshing of the structure must be performed. Calculation of the matrix elements, filling, and inversion of the impedance matrix is performed once. The impedance matrix can be re-used for each geometrical parameter and each right-hand side only needs N^2 computations if N is the number of unknowns. Port lines can be re-used during simulation. The approach treats all possible geometrical parameters in the plane of the circuit in a uniform way. Through the examples we saw that the integral equation calculated derivatives (IED) coincides well with their finite difference estimates (FDD). Moreover this IED is superior to the FDD if different grids are used for the perturbed geometries. In that case the FDD often exhibits nonphysical discontinuities.

Appendix
Derivation of an Integral Equation for the Geometrical Derivative of the Current

A. Vector Identities

We define a tensor as in [20]

$$\bar{\nabla}\bar{a} = \bar{u}_x\frac{\partial \bar{a}}{\partial x} + \bar{u}_y\frac{\partial \bar{a}}{\partial y} + \bar{u}_z\frac{\partial \bar{a}}{\partial z} = \bar{\nabla}a_x\bar{u}_x + \bar{\nabla}a_y\bar{u}_y + \bar{\nabla}a_z\bar{u}_z. \tag{53}$$

We formulate two vector identities in a suitable form. The first one concerns the gradient of the scalar product of two vector fields

$$\bar{\nabla}(\bar{a}\cdot\bar{b}) = \bar{a}\times(\bar{\nabla}\times\bar{b}) + (\bar{a}\cdot\bar{\nabla})\bar{b} + \bar{b}\times(\bar{\nabla}\times\bar{a}) + (\bar{b}\cdot\bar{\nabla})\bar{a}. \tag{54}$$

This identity (54) can be rewritten with tensor notations as

$$\bar{\nabla}(\bar{a}\cdot\bar{b}) = (\bar{\nabla}\bar{a})\cdot\bar{b} + (\bar{\nabla}\bar{b})\cdot\bar{a} \tag{55}$$

where the brackets cannot be omitted. By term wise identification of (54) and (55), one gets

$$(\bar{\nabla}\bar{b})\cdot\bar{a} = (\bar{a}\cdot\bar{\nabla})\bar{b} + \bar{a}\times(\bar{\nabla}\times\bar{b}) \tag{56}$$

and we will use the following alternative form of the identity (54)

$$\bar{\nabla}(\bar{a}\cdot\bar{b}) = (\bar{\nabla}\bar{a})\cdot\bar{b} + (\bar{a}\cdot\bar{\nabla})\bar{b} + \bar{a}\times(\bar{\nabla}\times\bar{b}). \quad (57)$$

For the second vector identity, we start from

$$\bar{\nabla}\times(\bar{a}\times\bar{b}) = \bar{a}(\bar{\nabla}\cdot\bar{b}) - \bar{b}(\bar{\nabla}\cdot\bar{a}) + (\bar{b}\cdot\bar{\nabla})\bar{a} - (\bar{a}\cdot\bar{\nabla})\bar{b}. \quad (58)$$

Or equivalently

$$(\bar{a}\cdot\bar{\nabla})\bar{b} = \bar{a}(\bar{\nabla}\cdot\bar{b}) - \bar{b}(\bar{\nabla}\cdot\bar{a}) + (\bar{b}\cdot\bar{\nabla})\bar{a} - \bar{\nabla}\times(\bar{a}\times\bar{b}). \quad (59)$$

Taking the divergence of both sides of (59), one gets

$$\bar{\nabla}\cdot[(\bar{a}\cdot\bar{\nabla})\bar{b}] = \bar{a}\cdot\bar{\nabla}(\bar{\nabla}\cdot\bar{b}) - \bar{b}\cdot\bar{\nabla}(\bar{\nabla}\cdot\bar{a}) + \bar{\nabla}\cdot[(\bar{b}\cdot\bar{\nabla})\bar{a}]. \quad (60)$$

B. The Flux Transport Theorem for Vector Fields

Given a vector field $\bar{F}$ and let $\bar{E}$ be the flux vector defined by

$$\bar{E} = \int_{S_\xi} \bar{F}\,dS \quad (61)$$

where the surface S_ξ depends on the parameter ξ, then the the total variation of $\bar{E}$ with respect to the parameter ξ is given by

$$\frac{\partial\bar{E}}{\partial\xi} + (\bar{v}\cdot\bar{\nabla})\bar{E} = \int_{S_\xi}\frac{\partial F}{\partial\xi} + \bar{\nabla}\cdot(\bar{v}\bar{F})dS \quad (62)$$

where $\bar{v} = d\bar{r}/d\xi$.

C. Derivation of a New Integral Equation for the Geometrical Derivative of the Surface Current

We start from the well-known MPIE. The scattered electrical field $\bar{E}^s(\bar{r})$ is written here as a sum of two contributions

$$\begin{aligned}\bar{E}^{\text{inc}}(\bar{r}) &= -\bar{E}^s(\bar{r})\\ &= \bar{E}^A(\bar{r}) - \bar{E}^V(\bar{r})\\ &= \bar{E}^A(\bar{r}) - \bar{\nabla}\phi^V(\bar{r})\end{aligned} \quad (63)$$

where the two parts are given by

$$\begin{aligned}\bar{E}^A(\bar{r}) &= \int_{S_\xi} G^A(\bar{r}\mid\bar{r}')\bar{J}(\bar{r}')dS'\\ \phi^V(\bar{r}) &= \int_{S_\xi} G^V(\bar{r}\mid\bar{r}')p(\bar{r}')dS'\end{aligned} \quad (64)$$

Deriving both sides with respect to the parameter ξ, gives

$$\begin{aligned}&\frac{\partial\bar{E}^{\text{inc}}(\bar{r})}{\partial\xi} + (\bar{v}\cdot\bar{\nabla})\bar{E}^{\text{inc}}(\bar{r})\\ &= \frac{\partial\bar{E}^A(\bar{r})}{\partial\xi} + (\bar{v}\cdot\bar{\nabla})\bar{E}^A(\bar{r}) - \frac{\partial\bar{E}^V(\bar{r})}{\partial\xi} - (\bar{v}\cdot\bar{\nabla})\bar{E}^V(\bar{r})\\ &= \frac{\partial\bar{E}^A(\bar{r})}{\partial\xi} + (\bar{v}\cdot\bar{\nabla})\bar{E}^A(\bar{r}) - \bar{\nabla}\frac{\partial\phi^V(\bar{r})}{\partial\xi} - (\bar{v}\cdot\bar{\nabla})\bar{\nabla}\phi^V(\bar{r})\end{aligned} \quad (65)$$

where $\bar{v} = d\bar{r}/d\xi = dx/d\xi\bar{u}_x + dy/d\xi\bar{u}_y$. Using the notations $p' = p(\bar{r}') = \bar{\nabla}'\cdot\bar{J}(\bar{r}')$, $\bar{J}' = \bar{J}(\bar{r}')$, introducing (64) in (65) and using the flux Theorem (62), we get

$$\begin{aligned}&\frac{\partial\bar{E}^{\text{inc}}(\bar{r})}{\partial\xi} + (\bar{v}\cdot\bar{\nabla})\bar{E}^{\text{inc}}(\bar{r})\\ &= \int_{S_\xi}[\bar{v}'\cdot\bar{\nabla}'G^A(\bar{r}\mid\bar{r}') + \bar{v}\cdot\bar{\nabla}G^A(\bar{r}\mid\bar{r}')\\ &\qquad + \bar{\nabla}'\cdot\bar{v}'G^A(\bar{r}\mid\bar{r}')]\bar{J}'\\ &\quad + G^A(\bar{r}\mid\bar{r}')\left[\frac{\partial\bar{J}'}{\partial\xi} + (\bar{v}\cdot\bar{\nabla})\bar{J}'\right]dS'\\ &\quad - \bar{\nabla}\left\{\int_{S_\xi}\bar{v}'\cdot\bar{\nabla}'G^V(\bar{r}\mid\bar{r}')p' + \bar{\nabla}'\cdot\bar{v}'G^V(\bar{r}\mid\bar{r}')p'\right.\\ &\qquad \left. + G^V(\bar{r}\mid\bar{r}')\left[\frac{\partial p'}{\partial\xi} + \bar{v}'\cdot\bar{\nabla}'p'\right]dS'\right\}\\ &\quad - (\bar{v}\cdot\bar{\nabla})\bar{\nabla}\left\{\int_{S_\xi}G^V(\bar{r}\mid\bar{r}')p'dS'\right\}.\end{aligned} \quad (66)$$

The last term can be rearranged by using the identity (57) with $\bar{a} = \bar{v}$ and $\bar{b} = \bar{\nabla}G^V(\bar{r}\mid\bar{r}')$

$$\begin{aligned}&\bar{\nabla}(\bar{v}\cdot\bar{\nabla}G^V(\bar{r}\mid\bar{r}'))\\ &\quad = (\bar{\nabla}\bar{v})\cdot\bar{\nabla}G^V(\bar{r}\mid\bar{r}') + (\bar{v}\cdot\bar{\nabla})\bar{\nabla}G^V(\bar{r}\mid\bar{r}')\end{aligned} \quad (67)$$

and this leads to

$$\begin{aligned}&\frac{\partial\bar{E}^{\text{inc}}(\bar{r})}{\partial\xi} + (\bar{v}\cdot\bar{\nabla})\bar{E}^{\text{inc}}(\bar{r})\\ &= \int_{S_\xi}[\bar{v}'\cdot\bar{\nabla}'G^A(\bar{r}\mid\bar{r}') - \bar{v}\cdot\bar{\nabla}'G^A(\bar{r}\mid\bar{r}')]\bar{J}'\\ &\quad + \bar{\nabla}'\cdot\bar{v}'G^A(\bar{r}\mid\bar{r}')\bar{J}' + G^A(\bar{r}\mid\bar{r}')\left[\frac{\partial\bar{J}'}{\partial\xi} + (\bar{v}\cdot\bar{\nabla})\bar{J}'\right]dS'\\ &\quad - \bar{\nabla}\left\{\int_{S_\xi}\bar{v}'\cdot\bar{\nabla}'G^V(\bar{r}\mid\bar{r}')p' - \bar{v}\cdot\bar{\nabla}'G^V(\bar{r}\mid\bar{r}')p'\right.\\ &\qquad + \bar{\nabla}'\cdot\bar{v}'G^V(\bar{r}\mid\bar{r}')p' + G^V(\bar{r}\mid\bar{r}')\\ &\qquad \left.\times\left[\frac{\partial p'}{\partial\xi} + \bar{v}'\cdot\bar{\nabla}'p'\right]dS'\right\} + (\bar{\nabla}\bar{v})\\ &\quad \cdot\bar{\nabla}\left\{\int_{S_\xi}G^V(\bar{r}\mid\bar{r}')p'dS'\right\}\end{aligned} \quad (68)$$

where we used the fact that $\bar{\nabla}G^V(\bar{r}\mid\bar{r}') = -\bar{\nabla}'G^V(\bar{r}\mid\bar{r}')$. Finally we rewrite the (68) as

$$\begin{aligned}&\frac{\partial\bar{E}^{\text{inc}}(\bar{r})}{\partial\xi} + (\bar{v}\cdot\bar{\nabla})\bar{E}^{\text{inc}}(\bar{r})\\ &= \int_{S_\xi}\bar{\nabla}'\cdot[(\bar{v}'-\bar{v})G^A(\bar{r}\mid\bar{r}')]\bar{J}'\\ &\quad + G^A(\bar{r}\mid\bar{r}')\left[\frac{\partial\bar{J}'}{\partial\xi} + (\bar{v}'\cdot\bar{\nabla}')\bar{J}'\right]dS'\\ &\quad - \bar{\nabla}\left\{\int_{S_\xi}\bar{\nabla}'\cdot[(\bar{v}'-\bar{v})G^V(\bar{r}\mid\bar{r}')]p'\right.\\ &\qquad \left. + G^V(\bar{r}\mid\bar{r}')\left[\frac{\partial p'}{\partial\xi} + \bar{v}'\cdot\bar{\nabla}'p'\right]dS'\right\}\\ &\quad + (\bar{\nabla}\bar{v})\cdot\bar{\nabla}\left\{\int_{S_\xi}G^V(\bar{r}\mid\bar{r}')p'dS'\right\}.\end{aligned} \quad (69)$$

The term $(\bar{v}' \cdot \bar{\nabla}')p'$ is fully rewritten as $\bar{v}' \cdot \bar{\nabla}'(\bar{\nabla}' \cdot \bar{J}')$. Using the vector identity (60) with $\bar{a} = \bar{v}'$ and $\bar{b} = \bar{J}'$, one gets

$$\bar{\nabla}' \cdot [(\bar{v}' \cdot \bar{\nabla}')\bar{J}'] = \bar{v}' \cdot \bar{\nabla}'(\bar{\nabla}' \cdot \bar{J}') - \bar{J}' \cdot \bar{\nabla}'(\bar{\nabla}' \cdot \bar{v}') + \bar{\nabla}' \cdot [(\bar{J}' \cdot \bar{\nabla}')\bar{v}']. \tag{70}$$

This means that

$$\partial p' \partial \xi + (\bar{v}' \cdot \bar{\nabla}')p' = \bar{\nabla}' \cdot \frac{\partial \bar{J}'}{\partial \xi} + \bar{\nabla}' \cdot [(\bar{v}' \cdot \bar{\nabla}')\bar{J}'] + \bar{J}' \cdot \bar{\nabla}'(\bar{\nabla}' \cdot \bar{v}') - \bar{\nabla}' \cdot [(\bar{J}' \cdot \bar{\nabla}')\bar{v}']. \tag{71}$$

Using this result (69) is rewritten as

$$\begin{aligned}
&\frac{\partial \bar{E}^{\mathrm{inc}}(\bar{r})}{\partial \xi} + (\bar{v} \cdot \bar{\nabla})\bar{E}^{\mathrm{inc}}(\bar{r}) \\
&= \int_{S_\xi} \bar{\nabla}' \cdot [(\bar{v}' - \bar{v})G^A(\bar{r} \mid \bar{r}')]\bar{J}' \\
&\quad + G^A(\bar{r} \mid \bar{r}')\left[\frac{\partial \bar{J}'}{\partial \xi} + (\bar{v}' \cdot \bar{\nabla}')\bar{J}'\right] dS' \\
&\quad - \bar{\nabla}\Bigg\{ \int_{S_\xi} \bar{\nabla}' \cdot [(\bar{v}' - \bar{v})G^V(\bar{r} \mid \bar{r}')]\bar{\nabla}' \cdot \bar{J}' \\
&\qquad + G^V(\bar{r} \mid \bar{r}')\bar{\nabla}' \cdot \left[\frac{\partial \bar{J}'}{\partial \xi} + (\bar{v}' \cdot \bar{\nabla}')\bar{J}'\right] \\
&\qquad + G^V(\bar{r} \mid \bar{r}')\bar{J}' \cdot \bar{\nabla}'(\bar{\nabla}' \cdot \bar{v}') - G^V(\bar{r} \mid \bar{r}')\bar{\nabla}' \\
&\qquad \cdot [(\bar{J}' \cdot \bar{\nabla}')\bar{v}']dS' \Bigg\} \\
&\quad + (\bar{\nabla}\bar{v}) \cdot \bar{\nabla}\left\{ \int_{S_\xi} G^V(\bar{r} \mid \bar{r}')\bar{\nabla}' \cdot J' dS' \right\}.
\end{aligned} \tag{72}$$

REFERENCES

[1] Jansen, "The spectral domain approach for MIC," *IEEE Trans. Microwave Theory Tech.*, vol. 33, pp. 1043–1056, 1985.

[2] Z. J Cendes, "The transfinite element method for modeling MMIC devices," *IEEE Trans Microwave Theory Tech.*, vol. 36, pp. 1639–1649, 1988.

[3] J R. Mosig, "Arbitrarily shaped microstrip structures and their analysis with a mixed potential integral equation," *IEEE Trans. Microwave Theory Tech*, vol 36, no 2, pp. 314–323, Feb. 1988

[4] J. X. Zheng, "Electromagnetic modeling of microstrip circuit discontinuities and antennas of arbitrary shape," Ph.D. dissertation, Univ. of Colorado-Boulder, 1990.

[5] J Bandler, R M. Biernacki, S. H. Chen, D. G. Swanson, and S. Ye, "Microstrip filter design using direct EM field simulation," *IEEE Trans. Microwave Theory Tech.*, vol. 42, no 7, pp 1353–1359, July 1994.

[6] J. Bandler, R. M Biernacki, S. H Chen, A P. Grobelny, and S. Ye, "Yield-driven electromagnetic optimization via multilevel multidimensional models," *IEEE Trans. Microwave Theory Tech.*, vol. 41, no. 12, pp. 2269–2278, Dec. 1993

[7] P. Garcia and J. P. Webb, "Optimization of planar devices by the finite element method," *IEEE Trans Microwave Theory Tech.*, vol. 38, no. 1, pp. 48–53, Jan 1990.

[8] J. W. Bandler, W. Kellermann, and K. Madsen, "A superlinearly convergent minimax algorithm for microwave circuit design," *IEEE Trans. Microwave Theory Tech.*, vol. 33, no. 12, pp. 1519–1530, Dec. 1985.

[9] R M. Biernacki, J. W. Bandler, J. Song, and Qi jun Zhang, "Efficient quadratic approximation for statistical design," *IEEE Trans. Microwave Theory Tech.*, vol 36, no 11, pp. 1449–1454, Nov. 1989.

[10] Z. A. Hafid, Q J Zhang, and M Nahkla, "Analysis and optimization of microwave circuits and devices using neural networks models," in *IEEE Microwave Theory Tech. Soc. Int. Symp Dig* , 1994, pp 393–396.

[11] T -S. Horng and C.-C. Wang, "Microstrip circuit design using neural networks," in *IEEE Microwave Theory Tech. Soc. Int. Symp. Dig.*, 1993, pp. 413–416.

[12] J. W. Bandler, R. M. Biernacki, S. H. Chen, P. A. Grobelny, and R. H. Hemmers, "Exploitation of coarse grid for electromagnetic optimization," in *IEEE Microwave Theory Tech. Soc. Int. Symp. Dig.*, 1994, pp. 381–384.

[13] F. Alesandri, M Mongiardo, and R Sorrentino, "New efficient full wave optimization of microwave circuits by the adjoint network method," *IEEE Microwave and Guided Wave Lett* , vol. 3, no 11, pp. 414–416, 1993

[14] F Alesandri, M. Dionigi, R. Sorrentino, and M Mongiardo, "A fullwave CAD tool of waveguide components using a high speed direct optimizer," in *IEEE Microwave Theory Tech Soc Int. Symp Dig* , 1994, pp. 1539–1542.

[15] J. Ureel and D. De Zutter, "Shape sensitivities of planar electrostatic problems using the method of moments," *IEEE Trans. Microwave Theory Tech.*, accepted for publication.

[16] ——, "Field-based sensitivities obtained with the method of moments for planar electrostatic problems," in *Proc. 1995 URSI Int. Symp. Electromagnetic Theory*, 1995, pp. 336–338

[17] J. Sercu, N Faché, F Libbrecht, and D. De Zutter, "Full-wave space-domain analysis of open microstrip discontinuities including the singular current-edge behavior," *IEEE Trans Microwave Theory Tech.*, vol 41, no 9, pp. 1581–1588, 1993.

[18] J. Sercu, N. Faché, and D. De Zutter, "Characterization of TEM and non-TEM planar transmission lines with a full-wave 3D field analysis technique," in *IEEE Microwave Theory . Soc. Int. Symp. Dig.*, 1993.

[19] P. George and T. Jilin, "Full-wave analysis of radiation effects of microstrip transmission lines," in *IEEE Antennas Propagat. Soc Int. Symp. Dig.*, 1993, pp. 626–629.

[20] J. Van Bladel, *Electromagnetic Fields,* 2nd ed New York Hemisphere, 1985

Jan Ureel (S'91) for a photograph and biography, see this issue, p. 207

Daniël De Zutter, (M'92) for a photograph and biography, see this issue, p. 207